J. Fluid Mech. (1982), *vol.* 120, *pp.* 411–431
Printed in Great Britain

Onset of convection in a variable-viscosity fluid

By KARL C. STENGEL, DEAN S. OLIVER AND JOHN R. BOOKER

Geophysics Program, University of Washington, Seattle, WA 98195, U.S.A.

(Received 27 March 1979 and in revised form 26 November 1981)

The Rayleigh number R_0 in a horizontal layer with temperature-dependent viscosity can be based on the viscosity at T_0, the mean of the boundary temperatures. The critical Rayleigh number R_{0c} for fluids with exponential and super-exponential viscosity variation is nearly constant at low values of the ratio of the viscosities at the top and bottom boundaries; increases at moderate values of the viscosity ratio, reaching a maximum at a ratio of about 3000, and then decreases. This behaviour is explained by a simple physical argument based on the idea that convection begins first in the sublayer with maximum Rayleigh number. The prediction of Palm (1960) that certain types of temperature-dependent viscosity always decrease R_{0c} is confirmed by numerical results but is not relevant to the viscosity variations typical of real liquids. The infinitesimal-amplitude state assumed by linear theory in calculating R_{0c} does not exist because the convection jumps immediately to a finite amplitude at R_{0c}. We observe a heat-flux jump at R_{0c} exceeding 10% when the viscosity ratio exceeds 150. However, experimental measurements of R_{0c} for glycerol up to a viscosity ratio of 3400 are in good agreement with the numerical predictions when the effects of a temperature-dependent expansion coefficient and thermal diffusivity are included.

1. Introduction

Convection in a horizontal fluid layer with isothermal boundaries and no internal heat sources is governed by the non-dimensional Rayleigh number

$$R = \frac{\alpha g \Delta T d^3}{\kappa \nu},$$

where α is the thermal expansion coefficient, g is the acceleration due to gravity, ΔT is the temperature drop from the bottom to the top of the layer, d is the layer depth, ν is the viscosity, $\kappa = k/\rho c_p$ is the thermal diffusivity, k is the thermal conductivity, ρ is the density and c_p is the specific heat. When the viscosity varies, defining the Rayleigh number requires an appropriate choice of viscosity. A widely used possibility introduced by Palm (1960) is ν_0, the viscosity at the mean of the boundary temperatures. The corresponding Rayleigh number is R_0. Other useful choices include $\tilde{\nu}$ the viscosity at the bottom, warm boundary and $\bar{\nu}$, the mean viscosity in the layer.

Accurate measurement of the critical Rayleigh number R_c for the onset of convection is never easy. It requires a sensitive method of determining when convection begins, accurate knowledge of the material properties, and accurate measurements of ΔT and d. Still, for constant-viscosity fluids, experimental determinations of R_c are in good agreement with linear theory (Schmidt & Milverton 1935; Silveston 1958).

For fluids with strongly temperature-dependent viscosity such as occur in many industrial and geophysical contexts, the infinitesimal amplitude convection assumed by linear theory should not exist. Instead the convection jumps to a finite-amplitude state and subcritical convection is possible (Busse 1967). Although linear theory is expected to predict R_{0c} accurately, few experimental results exist.

The only direct measurements of R_{0c} in fluids with significant viscosity variation are by Hoard, Robertson & Acrivos (1970) and Somerscales & Dougherty (1970). In both cases, the experimental fluids have viscosities that are greater when the fluids are cold and have steeper viscosity gradients at low temperatures. At a viscosity ratio between the top and bottom boundaries of about 10, Hoard *et al.* find a 12 % decrease in R_{0c} relative to a fluid with nearly constant viscosity. This is in reasonable agreement with a theoretical calculation by Liang (1969) using the actual viscosity variation of the experimental liquid used by Hoard *et al.* It also seems consistent with work of Palm (1960) and Jenssen (1963), who used a perturbation method to show that R_{0c} decreases for a fluid with a small cosine variation of viscosity.

The maximum viscosity ratio for the measurements of Somerscales & Dougherty is only about 2. Using the appearnce of the convective flow pattern as the criterion for onset, they find a decrease in R_{0c} in fair agreement with the predictions of Jenssen. However, using heat-transfer measurements to define the onset, they find an increase in R_{0c} as the viscosity ratio increases.

The only other observations of convective onset with strongly temperature-dependent viscosity are by Richter (1978). He does a study of flow structure at viscosity ratios up to 20, similar to the constant-viscosity work of Busse & Whitehead (1971). Richter measures the critical temperature differences across the layer but, since he does not have sufficient knowledge of the properties of his fluids, he calculates the Rayleigh number at higher temperature differences by assuming that $R_{0c} = 1707$ (the value for a constant-viscosity fluid with isothermal, no-slip boundaries). This procedure clearly gives no insight into the effect of the variable viscosity on R_c.

In the first part of this paper, we present theoretical calculations which disagree with Liang's result. For viscosity variations similar to Liang's, we find that R_{0c} initially increases with viscosity ratio. When the viscosity ratio exceeds about 3000, the onset of convection is governed by the development of a stable region over an unstable sublayer and R_{0c} decreases again. For the cosine viscosity variation, our calculations confirm the decrease in R_{0c} found by Palm and Jenssen, but demonstrate that at large viscosity ratio the structure of the convection is fundamentally different from the more realistic viscosity variations.

Since our predictions are in apparent conflict with the experiment of Hoard *et al.* (1970) and in partial conflict with the results of Somerscales & Dougherty (1970), and since the effect of the finite-amplitude convection at R_{0c} is unknown, further experimental verification is clearly desirable. The remainder of the paper presents results of an experiment to measure R_{0c} at viscosity ratios up to 3400. Our results are in good agreement with our theoretical predictions.

2. Calculation of R_c

In this section, dimensional variables are primed, constants and non-dimensional variables are unprimed. Constants and non-dimensional numbers with subscript zero are evaluated at the mean of the top and bottom boundary temperatures. We use the standard non-dimensionalization for convection studies modified for the fact that ν' and possibly α', k' and the heat capacity c_p' are temperature-dependent: length components $x_i' = dx_i$; time $t' = (d^2/\kappa_0)t$, where $\kappa = k/\rho c_p$; velocity components $u_i' = (\kappa_0/d)u_i$; temperature $T' = (\Delta T)T + T'_{\text{top}}$; viscosity $\nu' = \nu_0 f$; expansion coefficient $\alpha' = \alpha_0 A$; thermal conductivity $k' = k_0 K$, and heat capacity $c_p = c_{p0} Q$. We want to study a small perturbation $\tilde{\theta}$ to the linear, non-dimensional conductive temperature profile $\tilde{T} = 1 - x_3$. Note that the non-dimensional vertical co-ordinate is taken to be 0 at the bottom boundary and +1 at the top boundary. Thus, the mean of boundary temperatures is $T_0 = \frac{1}{2}$.

Using the Boussinesq approximation, the first-order equations for the perturbed quantities u_i, p (pressure) and $\tilde{\theta}$ are

$$\frac{\partial u_i}{\partial t} + \frac{\partial}{\partial x_i}\left(\frac{p}{\rho_0}\right) = R_0 A \tilde{\theta} \delta_{i3} + \frac{\partial}{\partial x_j}\left[f\left(\frac{\partial u_i}{\partial x_j} + \frac{\partial u_j}{\partial x_i}\right)\right], \tag{1}$$

$$\frac{\partial u_i}{\partial x_i} = 0, \tag{2}$$

$$\frac{\partial}{\partial t}(Q\tilde{\theta}) + u_i \frac{\partial}{\partial x_i}(Q\tilde{T}) = \frac{\partial}{\partial x_i}\left[K\left(\frac{\partial \tilde{\theta}}{\partial x_i}\right)\right], \tag{3}$$

where, according to convention, repeated subscripts imply summation with $\delta_{ij} = 1$ if $i = j$, 0 otherwise. Note that f, A, K and Q all multiply first-order terms containing u_i or $\tilde{\theta}$. Thus only the dependence of f, A, K and Q on the zeroth-order temperature $\tilde{T}$ enters the first-order equations. Since $\tilde{T}$ is a known function of x_3, f, A, K and Q are also known functions of x_3.

Pellew & Southwell (1940) prove for constant viscosity that the marginally stable state separating growing from decaying modes is time-independent. Their argument can easily be generalized to the variable-properties case. We therefore drop the time derivatives in (1) and (3). We then eliminate u_1, u_2 and p and seek a steady cellular solution

$$\tilde{\theta}(x_1, x_2, x_3) = \theta(x_3) \exp i(lx_1 + mx_2),$$

$$u_3(x_1, x_2, x_3) = W(x_3) \exp i(lx_1 + mx_2),$$

giving

$$R_0 A a^2 \theta = (D^2 f)(D^2 + a^2) W + 2(Df)(D^2 - a^2) DW + f(D^2 - a^2)^2 W, \tag{4}$$

where D denotes differentiation with respect to the vertical co-ordinate x_3, and $a^2 = l^2 + m^2$. Equation (3) becomes

$$K(D^2 - a^2)\theta + (D\theta)(DK) + [Q - DQ(1 - x_3)] W = 0. \tag{5}$$

In the case $A = K = Q = 1$, (4) and (5) yield

$$-R_0 a^2 \theta = (D^2 f)(D^4 - a^4)\theta + 2(Df)(D^2 - a^2)^2 D\theta + f(D^2 - a^2)^3 \theta, \tag{6}$$

which is equation (1) of Booker & Stengel (1978). In general, however, it is easier to work directly with the two equations (4) and (5).

We investigate three types of non-dimensional viscosity variation:

$$f = 1 - \gamma \cos \pi(1 - T), \tag{7}$$

$$f = \exp\left[c(\tfrac{1}{2} - T)\right], \tag{8}$$

$$f = \frac{1}{\nu_0} \exp F(T'), \tag{9}$$

where

$$0 \lesssim \gamma \lesssim 1, \quad c = \ln\left(\frac{\nu_{\max}}{\nu_{\min}}\right) = \ln \frac{1+\gamma}{1-\gamma} \tag{10}$$

(remember that the mean of the boundary temperatures $T_0 = \frac{1}{2}$). The function (7) is from Palm (1960) and Jenssen (1963) and is therefore called a Palm–Jenssen fluid. The function (8) is used by Torrance & Turcotte (1971) in their numerical study of finite-amplitude convection, and is called an exponential fluid. The function (9) is an empirical function derived from measurements of the viscosity of glycerol described in a later section.

For the Palm–Jenssen and exponential fluids, we assume that $A = K = Q = 1$. In order to compare our measurements in glycerol with theory, however, it is necessary to include the temperature dependence of A and Q. Fortuitously, K is essentially independent of temperature for glycerol (Newman 1968).

We consider two types of conditions on the top and bottom boundaries: no-slip, which implies $u_1 = u_2 = \theta = 0$ and stress-free, which implies $W = D^2 W = \theta = 0$. For convenience, we denote no-slip boundaries by R (rigid) and stress-free boundaries by F (free). We then use a fractional notation with the top of the fraction being the condition at the top boundary and the bottom of the fraction being the condition at the bottom boundary. Thus F/R means a stress-free top and a no-slip bottom. We consider four cases: F/F, R/R, F/R and R/F.

Equations (4) and (5) are easilytransformed into six first-order differential equations which can be numerically integrated by standard techniques. For a fixed horizontal wavenumber a, the boundary conditions can be satisfied only for certain values of the eigenvalue R_0. We use an iterative scheme described in detail by Stengel (1977) to find the R_0 that satisfies the boundary conditions. The initial guess in this scheme is always chosen to guarantee that we converge on the R_0 corresponding to the gravest vertical mode. The wavenumber a is then varied to find the absolute minimum R_0, which is R_{0c}, and its corresponding critical wavenumber a_c. The integrations are carried out on a CDC 6400 machine, and overall accuracy of R_{0c} is always more than three significant figures. At low viscosity ratio the accuracy of a_c is similar to R_{0c} but, at the largest ratios calculated, the dependence of R_{0c} on wavenumber becomes markedly weaker, and the accuracy of a_c is between two and three significant figures.

For small viscosity ratio (6) can be fairly easily solved for the F/F case using a second-order perturbation method (Stengel 1977). Although his calculation was done primarily to check the numerical results, it gives accurate values of R_{0c} for exponential fluids to the surprisingly high value of c greater than 5, corresponding to viscosity ratios greater than 150. His method will give accurate results for any fluid whose viscosity variation can be accurately represented by the first three terms in its power series, and is not limited to those whose viscosity decreases with increasing temperature.

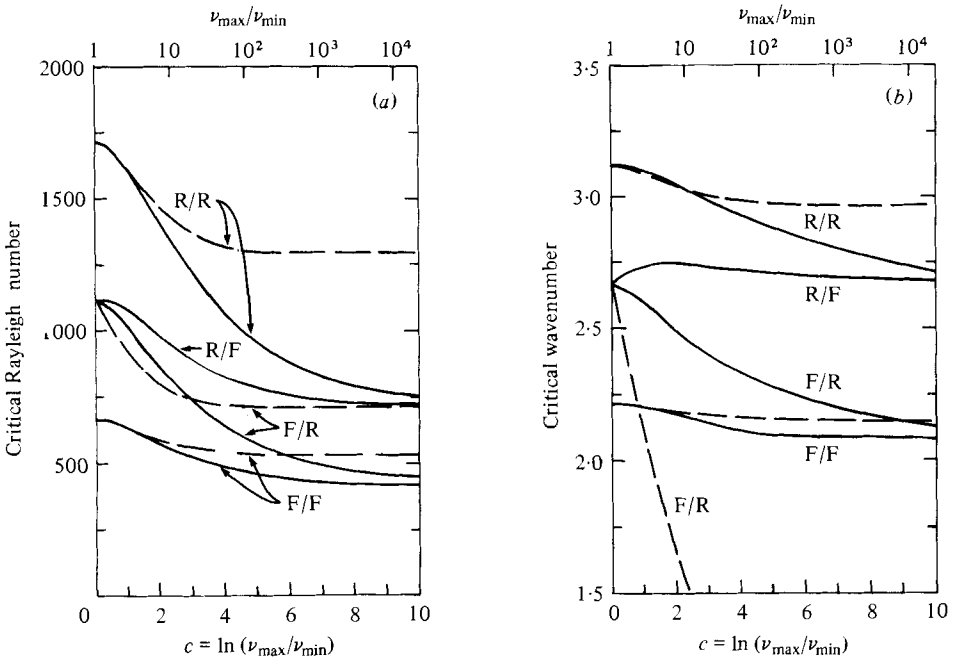

FIGURE 1. R_{0c} and a_c versus viscosity ratio for the Palm–Jenssen fluid. Solid lines are our numerical results. The dashed lines are perturbation results of Palm (1960) for F/F boundaries and Jenssen (1963) for F/R and R/R boundaries.

3. Numerical results

Figure 1 compares our numerical results for the F/F case with viscosity model (7) to Palm (1960) and for the R/R and F/R cases to Jenssen (1963). The R/F case, which has not been studied previously, is included for completeness. As one might expect, the perturbation and numerical results agree for small viscosity ratios, but diverge at higher values. In summary, Palm–Jenssen fluids show a decrease in R_{0c} and in a_c for almost all boundary conditions as the viscosity ratio increases. Only in the R/F case does a_c show an initial small increase which is followed by a decline. Note that Jenssen's prediction for a_c in the F/R case appears to be very poor except at very small viscosity ratio. This is unfortunate because his result might have been used to predict large horizontal stretching of cells in the Earth if convection were confined to the upper mantle. The failure of Jenssen's F/R calculation at very small viscosity ratios is not entirely unexpected, because it is only good to first order in γ, while the perturbation theories for the R/R and F/F cases are good to second order in γ.

The results for exponential fluids plotted in figure 2 are quite different from Palm–Jenssen fluids except at low viscosity ratio. Three regimes can be distinguished: (i) low viscosity ratio ($c \lesssim 1{\cdot}5$; $\nu_{max}/\nu_{min} \lesssim 5$) – R_{0c} and a_c are nearly constant; (ii) moderate viscosity ratio ($1{\cdot}5 \lesssim c \lesssim 8$; $5 \lesssim \nu_{max}/\nu_{min} \lesssim 3000$) – R_{0c} increases and a_c is nearly constant or decreases moderately depending on the boundary conditions; (iii) large viscosity ratio ($c \gtrsim 8$; $\nu_{max}/\nu_{min} \gtrsim 3000$) – R_{0c} reaches a peak and then decreases, while a_c rises rapidly. For large viscosity ratio, the layers with stress-free top boundaries (F/F and F/R) seem to forget that their highly viscous tops are free and both R_{0c} and a_c approach the corresponding case with a no-slip top boundary.

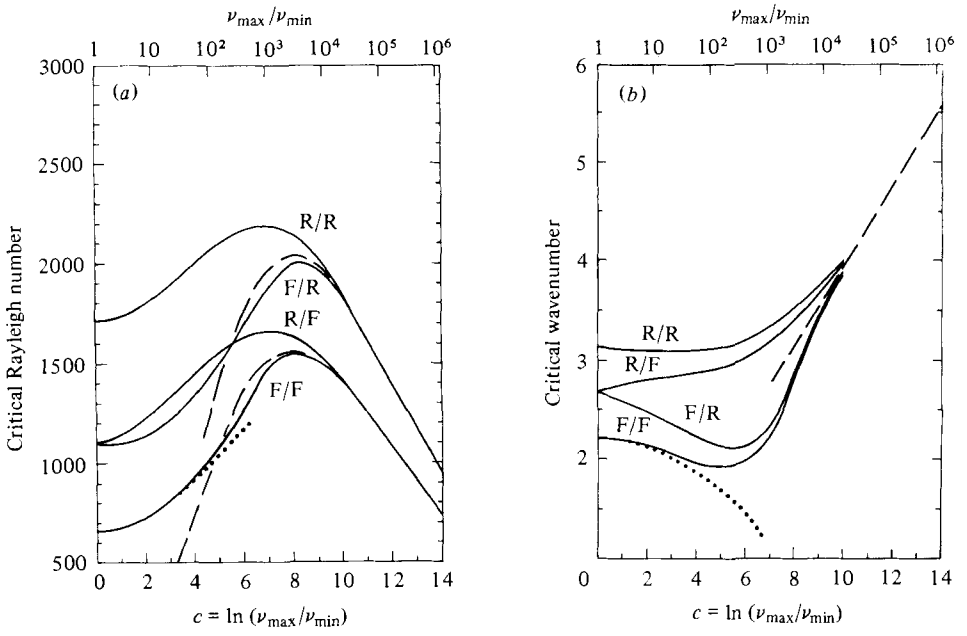

FIGURE 2. R_{0c} and a_c versus viscosity ratio for the exponential fluid. Solid lines are our numerical results; the dashed lines are for the approximate physical argument and the dotted line is from the perturbation calculation of Stengel (1977).

Note that the Palm–Jenssen fluids seem to have the opposite behaviour. As the viscosity ratio for the exponential fluid increases further, R_{0c} eventually drops below the value it takes in a constant-viscosity fluid, and a_c for all types of boundaries converges to a single line with a_c directly proportional to c.

Figure 3 gives results for the glycerol viscosity variation (9) assuming that $T_0 = 20\,^{\circ}\mathrm{C}$ and $A = Q = K = 1$. Only the experimentally important R/R and F/R cases were calculated. The behaviour is similar to the exponential fluid, although the magnitude of the increase in R_{0c} is considerably larger and the viscosity ratio at the peak is slightly higher. The convergence of the results for the two types of upper boundaries still occurs at large viscosity ratio, although a_c does not appear to be converging to a direct dependence on c.

4. Discussion of theoretical results

Most of our numerical results can be explained by a simple physical model which postulates that convection begins in the sublayer with maximum Rayleigh number. For fluids with $\partial f/\partial T < 0$, it is easy to show that this sublayer must extend to the bottom boundary. Then the Rayleigh number of a sublayer that extends from the base of the fluid to a height $\hat{d} = \hat{z}d$ is

$$\hat{R}_0 = \frac{\alpha g \beta (\hat{z}d)^4}{\kappa \nu(\hat{T}_0)} = R_0 \frac{\hat{z}^4}{f(\hat{T}_0)}, \tag{11}$$

where $\beta = \Delta T/d$ is the conductive temperature gradient, $\hat{T}_0 = 1 - \frac{1}{2}\hat{z}$ is the mean of the sublayer boundary temperatures, and α and κ are assumed constant.

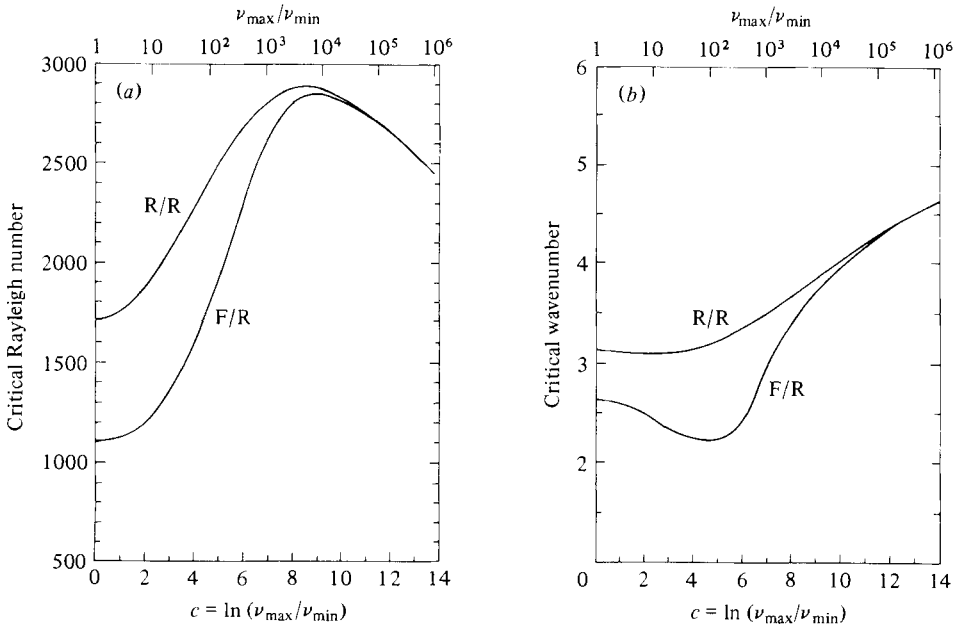

FIGURE 3. R_{0c} and a_c versus viscosity ratio for glycerol with $T_0 = 20$ °C.

We can now ask whether $\hat{R}_0$ can be larger than R_0. Differentiating (11) gives

$$\frac{\partial \hat{R}_0}{\partial \hat{z}} = \hat{R}_0 \left(\frac{4}{\hat{z}} - \tfrac{1}{2}c\right). \tag{12}$$

For $c < 8$ there is no $\hat{z} < 1$ for which $\partial \hat{R}_0/\partial \hat{z} \leqslant 0$. Thus $\hat{R}_0$ is maximum at $\hat{z} = 1$ and equals R_0. One would therefore expect the initial instability to extend throughout the layer. For $c > 8$, however, $\hat{R}_0$ will be maximum when

$$\hat{z} = 8/c, \tag{13}$$

and will exceed R_0. Convection should then begin in a sublayer which does not extend to the upper boundary. The log viscosity ratio of this sublayer is constant and is easily shown to be $\hat{c} = \hat{z}c = 8$.

One can also show that $\hat{R}_{0c}$ is constant at large c. Substituting (8) in (11) and using (13) gives

$$\hat{R}_0 = R_0 \left(\frac{8}{c}\right)^4 e^{\frac{1}{2}(c-8)}. \tag{14}$$

Therefore

$$\hat{R}_0 = 75{\cdot}02 R_0 c^{-4} e^{\frac{1}{2}c} \equiv 75{\cdot}02 \tilde{R}. \tag{15}$$

Figure 4 shows that the numerical values of $\tilde{R}_c$ converge to 27·5 ($\hat{R}_{0c} = 2038$) when the lower boundary is rigid, and 20·9 ($\hat{R}_{0c} = 1568$) when the lower boundary is free. Solving (15) for R_0 and using the asymptotic values of $\hat{R}_{0c}$ gives the dashed curves in figure 2. These curves are identical with the numerical results for $c > 10$ and predict the general shape of the numerical curves for $c > 5$.

Finally, one can show that the structure of the incipient flow is constant with

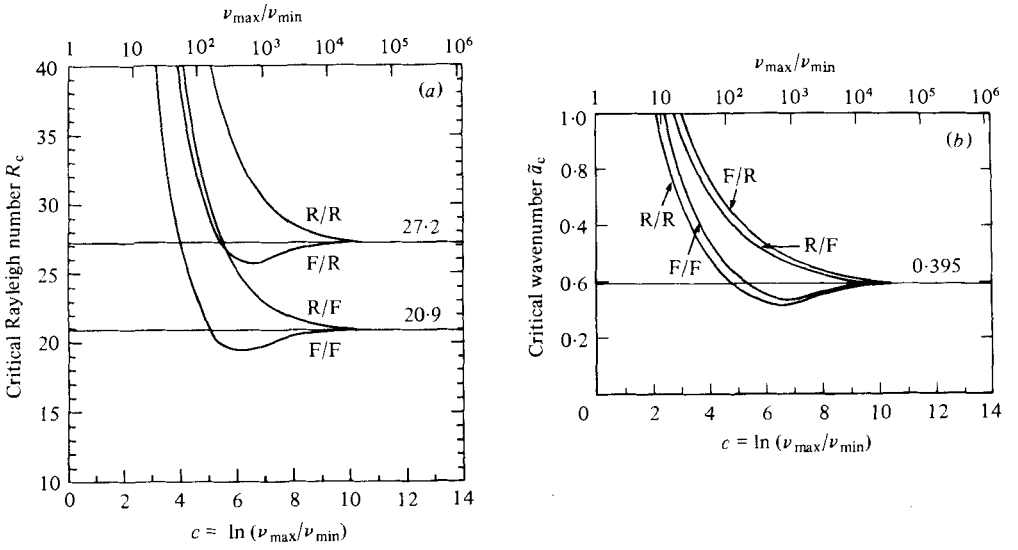

FIGURE 4. R_c (*a*) and $\tilde{a}_c$ (*b*) versus viscosity ratio for the exponential fluid. The horizontal lines are drawn at and labelled with the asymptotic values at large viscosity ratio.

respect to the sublayer depth. In the horizontal direction, the wavenumber non-dimensionalized by $\hat{d}$ is

$$\hat{a} = \hat{z}a = 8\left(\frac{a}{c}\right) \equiv 8\tilde{a}. \tag{16}$$

Figure 4 shows that $\tilde{a}_c$ converges to $0{\cdot}395 \pm 0{\cdot}005$ as c becomes large. The line $a_c = 0{\cdot}395c$ is shown in figure 2. The asymptotic value of $\hat{a}_c$ is therefore $3{\cdot}16 \pm 0{\cdot}04 \approx \pi$. Thus the half-wavelength of the convective motion in the sublayer is always equal to the depth of the sublayer.

In the vertical direction one could show that the eigenfunctions stretched by a factor $1/\hat{z}$ are identical for large values of c. However, a simple measure of vertical similarity which is independent of $\hat{z}$ is an intrinsic aspect ratio $\alpha_c z_p$, where z_p is the non-dimensional position of the peak of the vertical velocity eigenfunction (see figure 6). If the stretched eigenfunctions are identical, $z_p/\hat{z}$ must be constant, and the constancy of $\alpha_c z_p$ follows directly from (16). Figure 5 shows that $\alpha_c z_p$ in the R/R case converges to 0·711 for $c > 8$. An immediate consequence is that

$$z_p = 0{\cdot}225\hat{z} = 1{\cdot}80/c.$$

An interesting sidelight is that

$$2z_p = e^{-\frac{1}{10}c} = \left(\frac{\nu_{max}}{\nu_{min}}\right)^{-\frac{1}{10}}$$

fits all the numerical results for $c < 12$. The two relations are virtually identical for $8 < c < 12$.

The constancy of $\hat{c}$, $\hat{R}_{0c}$, $\hat{a}_c$ and $\alpha_c z_p$ at large c is to be expected if the fluid over the sublayer is stagnant. One can then increase c by adding stagnant fluid to the top of a marginal stable layer, keeping the temperature gradient β constant. The additional stagnant fluid will not affect the structure of the sublayer or the fact that it is marginally stable. That the stagnation actually happens is clear from comparison of the vertical

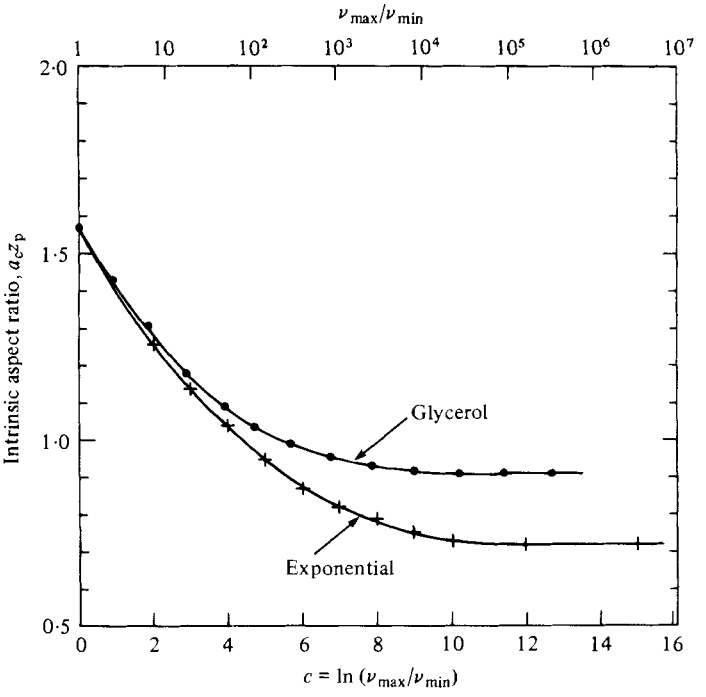

FIGURE 5. The intrinsic aspect ratio is the wavenumber a_c times the position of the peak of the vertical velocity eigenfunction z_p. At constant viscosity $a_c z_p = \frac{1}{2}\pi$. Crosses are the exponential fluid and solid circles are glycerol with $T_0 = 20$ °C. The boundaries are R/R.

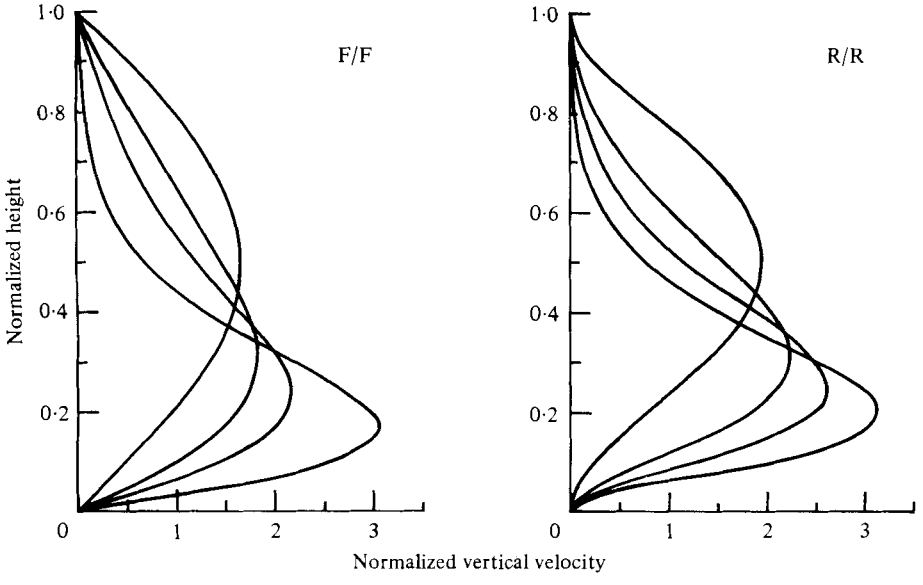

FIGURE 6. Vertical velocity eigenfunctions for F/F and R/R boundaries with $c = 0$, 5, 7 and 9 for the exponential fluid. The peak moves down in the layer as c increases. Note that the horizontal velocity eigenfunctions are proportional to the vertical derivative of these vertical velocity eigenfunctions. Thus as c increases, the horizontal velocity at the free upper boundary becomes small.

velocity eigenfunctions for the F/F and R/R cases plotted for increasing values of c in figure 6. At $c = 9$, the eigenfunctions are virtually identical in the top half of the layer for both rigid and free boundaries. Furthermore, the vertical derivatives of the eigenfunctions are very small near the upper boundary so that both the horizontal velocity and temperature eigenfunction are small in the stagnant lid. Consequently the boundary conditions at the top of the sublayer are essentially rigid and isothermal regardless of the actual conditions at the top of the layer. This explains the convergence of the R_{0c} curves for rigid and free top boundaries in figure 2.

The Rayleigh number $\tilde{R}$ has a simple physical meaning. Substituting for R_0 in (15) we get

$$\tilde{R} = \frac{\alpha g \beta (d/c)^4}{\kappa \nu_0 \exp(-\frac{1}{2}c)}.$$

Thus $\tilde{R}$ is the Rayleigh number based on a depth $\tilde{d} = d/c$ and a viscosity

$$\tilde{\nu} = \nu_0 \exp(-\tfrac{1}{2}c).$$

It is easy to show that $\tilde{d}$ is the scale depth for viscosity variations in the presence of the conductive temperature profile $\tilde{T}$ and $\tilde{\nu}$ is the viscosity at the bottom, warm boundary. Note also that $\tilde{d} = \frac{1}{8}\hat{d}$, and that $\tilde{a}$ is the wavenumber non-dimensionalized by $\tilde{d}$. $\tilde{R}$ and $\tilde{a}$ are obviously convenient definitions of the Rayleigh number and wavenumbers at very large viscosity ratio in exponential fluids because their critical values are independent of c. This result is closely related to the work of Schubert, Turcotte & Oxburgh (1969), who found for a semi-infinite fluid with a viscosity that increases exponentially downwards that $\tilde{R} = 30$ for a rigid top boundary and 23 for a free top.

A sublayer should form in glycerol in essentially the same way as in the exponential fluid. Using the empirical viscosity function for glycerol with $T_0 = 20\,^{\circ}\mathrm{C}$, there is a solution to $\partial \hat{R}_0/\partial \hat{z} = 0$ with $\hat{z} < 1$ when $\Delta T > 86{\cdot}9\,^{\circ}\mathrm{C}$ corresponding to $c > 8{\cdot}60$. This agrees well with c at the maximum R_{0c} in figure 3, and figure 4 demonstrates that the intrinsic aspect ratio $a_c z_p$ becomes constant at large c. However, $\hat{z}$ is a complicated function of c, and therefore $\hat{R}_0$, $\hat{a}$ and z_p will not converge to simple relations like (13)–(16). One can calculate the scale depth $\tilde{d}$ of the viscosity variation at the base of a glycerol layer and use it to define $\tilde{R}$ and $\tilde{a}$. However, neither becomes constant at large c and they are clearly not as useful as for exponential fluids.

It is clear from (12) that formation of a sublayer requires

$$\left(-\frac{1}{f}\frac{\partial f}{\partial T}\right)_{T=\frac{1}{2}} > 8.$$

This condition is never satisfied for the Palm–Jenssen fluid. Regardless of the viscosity ratio we would not expect a stagnant lid with the convection squeezed into a sublayer much thinner than the vertical scale of the layer, or the convection wavenumber to become much larger than at constant viscosity. There is also no basis for expecting $\tilde{R}$ to be useful for Palm–Jenssen fluids because $\tilde{d} = 0$. In fact, it is clear from figure 1 that it is R_{0c} that becomes constant as c becomes large.

The contrast between Palm–Jenssen and exponential fluids is further illustrated by the eigenfunctions for $c = 10$ in figures 7 (a, b). Figure 7 (a) compares the F/F case for the two types of fluid. Despite the large viscosity ratio, the horizontal velocity at the top boundary of a Palm–Jenssen fluid is almost as large as for a constant-viscosity

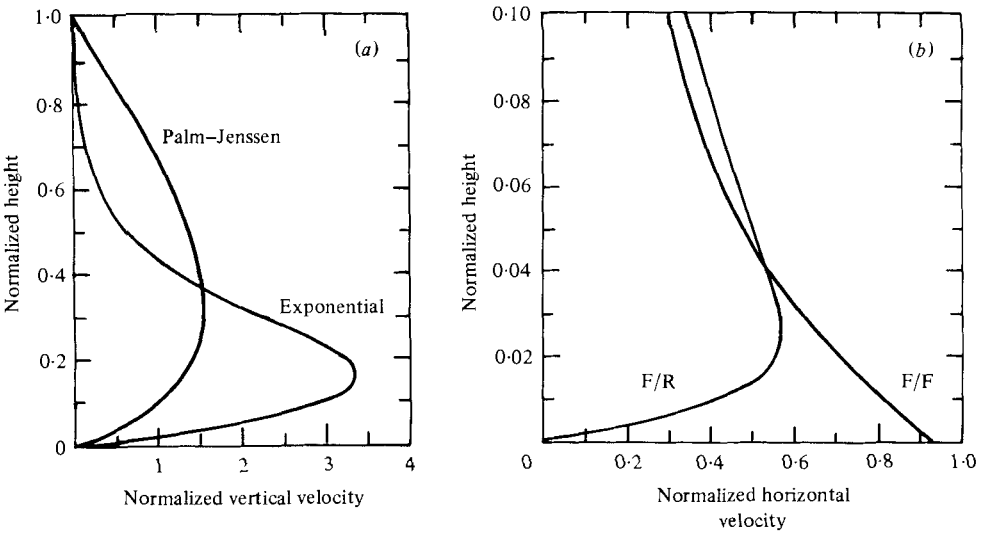

FIGURE 7. (*a*) A comparison of the vertical-velocity eigenfunctions for the Palm–Jenssen and exponential fluids with F/F boundaries and $c = 10$. The vertical derivative of these functions is proportional to the horizontal velocity. Note that the horizontal velocity at the top boundary is large for the Palm–Jenssen fluid and very small for the exponential fluid. Note also that the peak of the eigenfunction is much lower in the exponential fluid layer. Compare the Palm–Jenssen eigenfunction to the $c = 0$, F/F case in figure 4. (*b*) A comparison of the horizontal-velocity eigenfunctions for the Palm–Jenssen fluid with F/R and F/F boundaries and $c = 10$. Note that only the bottom 10% of the layer is shown. The eigenfunctions are nearly identical throughout the rest of the layer. The accommodation to the lower rigid boundary occurs in the bottom 2% of the layer.

fluid. Figure 7(*b*) is the horizontal velocity eigenfunction near the bottom boundary for the F/F and F/R cases in a Palm–Jenssen fluid. The functions are very similar except in a boundary transition region occupying only 2% of the total layer thickness. This is evidently why a Palm–Jenssen fluid seems to forget a rigid bottom boundary at large viscosity ratio.

Finally, an obvious alternative definition of the Rayleigh number is $\bar{R}$, using the mean viscosity $\bar{\nu}$ in the fluid layer. For Palm–Jenssen fluids, $\bar{\nu} = \nu_0$ and $\bar{R} = R_0$. For the exponential fluid,

$$\bar{\nu} = \nu_0 \frac{\sinh \frac{1}{2}c}{\frac{1}{2}c},$$

and $\bar{R} = (\nu_0/\bar{\nu})R_0$. $\bar{R}_c$ and R_{0c} for Palm–Jenssen and exponential fluids with F/F boundaries are plotted together in figure 8. Three things are evident: $\bar{R}_c$ decreases for both fluids; at small viscosity ratio ($c \lesssim 1$) $\bar{R}_c$ is more constant than R_{0c}; and at large viscosity ratio $\bar{R}_c$ decreases rapidly, showing no evidence of the structure in R_{0c} associated with the formation of the sublayer. At large c, $\bar{\nu}$ is heavily weighted by the viscosity in the stagnant lid. Thus it is obvious that $\bar{R}$ is not a very relevant parameter. At small c, $\bar{R}$ is clearly useful. In general, however, the slight advantage of $\bar{R}$ over R_0 at small c is probably outweighed by the difficulty of calculating $\bar{R}$.

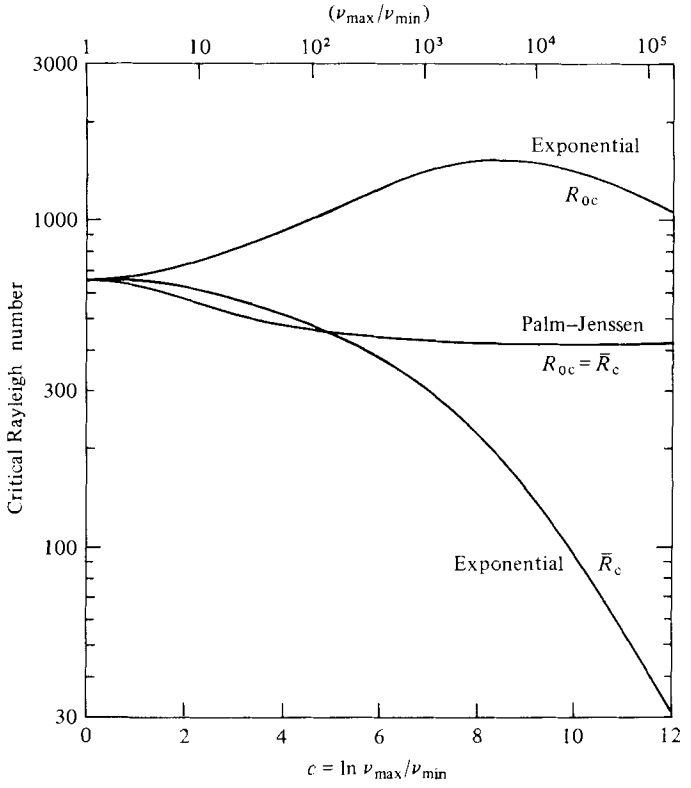

FIGURE 8. R_{0c} and $\bar{R}_c$ versus viscosity ratio for Palm–Jenssen and exponential fluids with F/F boundaries.

5. Apparatus

The viscosity ratio of 10 reached by Hoard *et al.* (1970) is really rather small. At $c = 2{\cdot}3$ (viscosity ratio = 10), we predict only a 5 % increase in R_{0c}, which would be very difficult to detect (see figure 3). The roughly 50 % increase in R_{0c} predicted at a viscosity ratio of 10^3, however, should be much easier to measure.

To achieve large viscosity variations within a reasonable temperature range, we use anhydrous glycerol as the working fluid. The viscosity of anhydrous glycerol varies by a factor of 4200 between + 70 and − 20 °C. The freezing point of pure glycerol is about + 18 °C, but it passes into a supercooled, glassy state below 18 °C with no decrease in specific heat and continuous variation of other properties. Transition to an amorphous solid with release of latent heat requires cooling to below − 50 °C. The ease of obtaining glycerol in a highly pure form, its safety as a laboratory fluid, its good optical transmission, and the comprehensive literature on its properties (Newman 1968) are considered sufficient compensation for the experimental problems that arise because of its hygroscopic nature.

The fluid layer in our circular apparatus is 26 cm in diameter and 1·2 cm thick giving an aspect ratio of 22: 1. This is an uncomfortably small aspect ratio, but it seems to be a necessary compromise for large viscosity ratios. The size is dictated by the dissipation capacity of our refrigeration system at − 20 °C. An aspect ratio of 80: 1 such as used in the high-quality structure studies for constant viscosity by Busse &

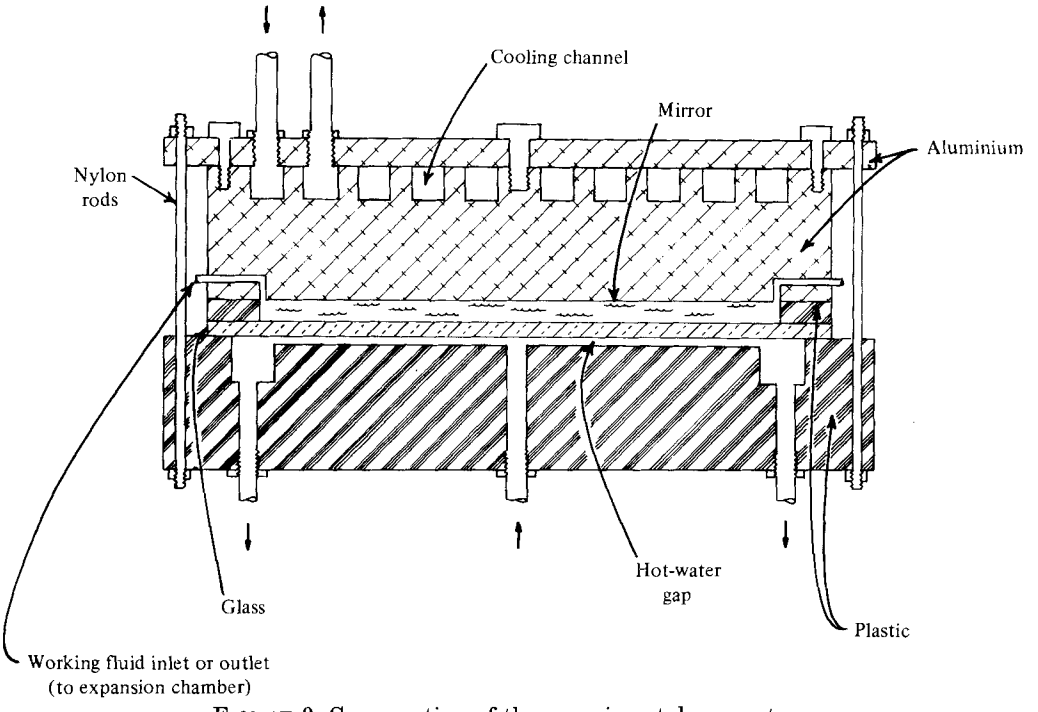

FIGURE 9. Cross-section of the experimental apparatus.

Whitehead (1971) and for small viscosity ratios by Richter (1978) would require dissipating 6 kW at -20 °C, a difficult and extremely expensive proposition.

A cross-section of the apparatus is shown in figure 9. The top plate is aluminium which has been polished flat by the techniques used to make telescope mirrors and then nickel-plated to give a highly reflecting surface. Ethyl alcohol cooled by the refrigerator circulates in a spiral trough milled in the top plate. Lateral temperature variations at the top of the fluid layer are less than $10^{-5}\Delta T$. The bottom plate is a sandwich of Pyrex glass and Plexiglas separated by a very thin gap. Hot fluid from a circulating bath enters at the centre of the Plexiglas plate and flows in the gap to a trough cut in the Plexiglas at the perimeter of the cell. The dimensions of the trench are such that the pressure gradient in it is small compared to the gap. This ensures radial flow of the heating fluid. The temperature drop between the centre and perimeter of the bottom boundary is about $10^{-3}\Delta T$.

The plastic ring that confines the glycerol laterally is 1·2 cm thick and 1·75 cm wide. It extends well into the region heated by the circulating fluid so that the vertical temperature profile on the inside edge of the ring closely matches the linear conductive profile in the glycerol. Thus the wide ring isolates the fluid layer from temperature inhomogeneities near the edge of the apparatus without the severe loss of aspect ratio entailed by a separate isolation ring in the interior of the fluid.

The temperature of the top boundary is measured to $\pm 0{\cdot}1$ °C with a copper–constantan thermocouple referenced to a commercial ice-point cell. In an initial series of experiments, the temperature at the boundary was measured using a thermocouple glued to the top of the glass plate. In a subsequent series intended primarily to measure heat transport, the thermocouple was replaced with a 0·025 mm diameter platinum

wire along a diameter of the cell and the temperature was determined to $\pm 0{\cdot}3\,^{\circ}\mathrm{C}$ from the wire's resistance. The platinum wire is much thinner than the thermocouple and has the additional advantage of spatially averaging the boundary temperature.

For the heat-transport measurements, the temperature in the circulating fluid gap was also measured with a thermocouple. The heat transport was then calculated from the temperature drop through the bottom plate. The conductivity of the plate was measured by comparing the temperature drop through the glass to quartz in a geometry where the heat flow through the glass and quartz was the same.

Parallel or slightly divergent light shines in the bottom of the cell, passes up through the convecting fluid, is reflected, passes again through the convecting fluid and thence out of the bottom to a glazed screen. Cold regions in the glycerol focus the light and warm regions defocus it, giving a 'shadowgraph' picture of the convection pattern. The added complication of a reflecting top plate is critical in obtaining large viscosity ratios because we are operating near the capacity of the cooling system. The temperature drop across a less-conducting glass top would significantly increase the minimum top-boundary temperature.

Anhydrous glycerol is extremely hygroscopic, and to maintain its very strong viscosity variation one must take special precautions to exclude water from the cell. To do this, we initially fill the cell with dry nitrogen. The glycerol then displaces the gas as the cell is filled while slightly tilted. A flexible expansion bottle partially filled with glycerol is connected at all times to the cell to compensate for volume changes which can occur when the cell is placed in operation. The fluid and expansion bottle are maintained at a slightly positive pressure, which prevents bubbles forming in the convecting layer if the glycerol contracts, discourages leakage of water into the apparatus, and compensates for the positive pressure created by the circulating pump, thus reducing flexure of the bottom glass plate. Measurement of the viscosity before and after a run confirms that no water contamination has occurred.

6. Properties of glycerol

Based on the data compiled in Newman (1968), our best estimates of the properties other than viscosity of anhydrous glycerol in the temperature range $T = 0$–$50\,^{\circ}\mathrm{C}$ are:

$$\alpha = [47 \pm 1 + 0{\cdot}2(T-20)] \times 10^{-5} \quad (^{\circ}\mathrm{C}^{-1}), \tag{17}$$

$$\rho = 1{\cdot}261\,34\,[1-(47\times 10^{-5})\,(T-20)] \quad (\mathrm{g\,cm^{-3}}),$$

$$1/\kappa = 1002 \pm 25 + 2{\cdot}78T \quad (\mathrm{s\,cm^{-2}}),$$

$$c_p = (54 \pm 0{\cdot}5 + 0{\cdot}15T) \times 10^{-2} \quad (\mathrm{cal\,g^{-1}}), \tag{18}$$

$$k = (68 \pm 1) \times 10^{-5} \quad (\mathrm{cal\,cm^{-1}\,s^{-1}\,^{\circ}C^{-1}}).$$

The stated uncertainties are valid throughout the temperature range, with the exception of the thermal expansion coefficient α. The temperature derivative of α is the second derivative of ρ, and is extremely difficult to determine accurately. Based on several types of data in Newman (1968), a minimum range for the temperature coefficient in (17) is 0·15–0·3. The uncertainty in ρ is not given because it is estimated to be much less than 1 %.

The source of the usual standard tables of the viscosity of glycerol (and its aqueous

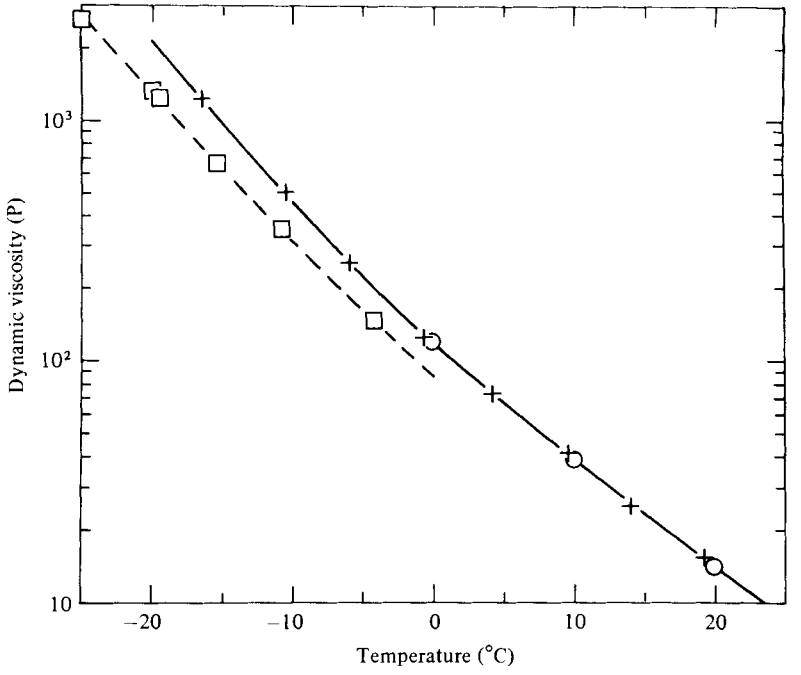

FIGURE 10. Dynamic viscosity of anhydrous glycerol versus temperature. The crosses are our measurements with a cone–plate viscometer. The open circles are from Segur & Oberstar (1951). The open squares are from Tamman & Hesse (1926). The solid curve is from the empirical relation (23).

T (°C)	η (P)	T (°C)	η (P)
−16·5	1220	19·3	15·0
−10·6	501	20	14·1
−6·0	256	30	6·10
−0·6	128	40	2·83
0	120	50	1·42
4·2	73·3	60	0·811
9·1	42·0	70	0·504
10	38·9	80	0·318
14·0	25·1	90	0·212

TABLE 1. Measured value of the dynamic viscosity of anhydrous glycerol. The values at 0, 10, 20 °C and higher are from Segur & Oberstar (1951), corrected for a viscosity of water equal to 0·01002 P at 20 °C.

solutions) in the temperature range from 0–100 °C (e.g. Newman 1968) is Segur & Oberstar (1951). They used capillary viscometers carefully corrected for effects of temperature on the calibration. Below 0 °C, the only major study of the viscosity of anhydrous glycerol is by Tamman & Hesse (1926) (compiled in Newman 1968). They use a falling-ball viscometer. Data between −25 and +20 °C from the two sources are plotted in figure 10. At 0 °C, these data are clearly inconsistent. Tamman & Hesse's predicted viscosity is 27 % below Segur & Oberstar's.

We have re-measured the viscosity of spectral-quality pure glycerol throughout the

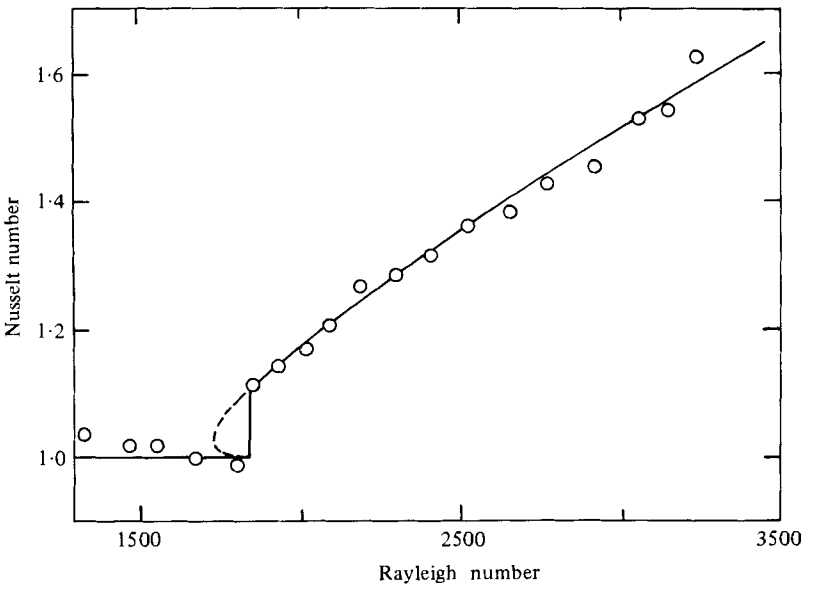

FIGURE 11. Heat flux in a fluid with large viscosity variation (c = 5·0). The circles are experimental points. The curve is a theoretical fit of Oliver (1980, 1982). The vertical part of the theoretical curve is drawn at R_0^*, the Rayleigh number at which the convective pattern would first be observed optically, deduced from a separate series of experiments.

experimental temperature range using a cone–plate viscometer. The viscometer is calibrated against a silicone-oil viscosity standard and is immersed in a dry nitrogen atmosphere. Our data below 20 °C are listed in table 1 and plotted in figure 10. Within the ± 2 % error of our measurements, our data are in agreement with Segur & Oberstar above 0 °C. Our measured point at − 16·5 °C is 56 % above the viscosity interpolated from Tamman & Hesse at this temperature. Since our subzero data join smoothly onto the results above 0 °C, we conclude that Tamman & Hesse must be systematically in error. Finally, after converting from dynamic to kinematic viscosity, the curve

$$\nu = \exp(4{\cdot}5490 - 0{\cdot}12309T + 9{\cdot}1129\times10^{-4}T^2 - 4{\cdot}7562\times10^{-4}T^3 + 1{\cdot}3296\times10^{-8}T^4) \qquad (19)$$

fits all the data in table 1 within ± 2 %.

7. Experimental results

Whenever the material properties of the fluid depend on temperature the possibility of subcritical finite-amplitude instabilities (Busse 1967) must be considered in the experimental procedure. Figure 11 shows the expected parabolic form of the relation between the Rayleigh number and the Nusselt number N (ratio of total heat transport to conductive heat transport). For increasing R_0, N should follow the solid line with a finite jump at R_{0c}. For decreasing R_0, N will follow the dashed curve until it reaches the minimum R_0 at which a finite-amplitude disturbance is possible, where N will jump back to 1. To avoid this hysteresis, we always approach R_{0c} from below.

A typical run involves increasing the bottom-boundary temperature in steps of 0·2–0·5 °C. This strategy keeps c nearly constant as R_0 increases. A more desirable strategy of increasing the layer depth with ΔT fixed is experimentally intractable, and an alternative strategy of decreasing the top temperature causes c to vary rapidly with

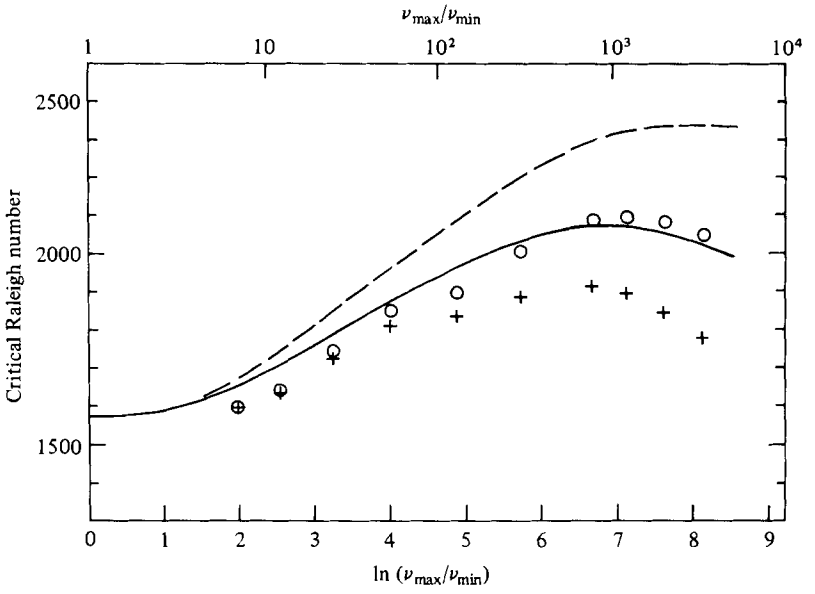

FIGURE 12. The crosses are measured values of R_0^*, the Rayleigh number at which the convection pattern is first observed optically. The circles are values of the critical Rayleigh number R_{0c} obtained by correcting R_0^* for the effect of the jump in Nusselt number on the boundary temperatures. The theoretical curves use the actual experimental boundary conditions. The solid curve assumes α and c_p vary with temperature according to (17) and (18). The dashed curve assumes α and c_p constant.

ΔT. The equilibration time for the heating and cooling units is approximately equal to the thermal time constant of the fluid layer, and we wait about ten times the layer time constant before proceeding to the next step. The curvature and rate of change of the temperature profile are small enough that they should have a negligible effect on R_c even at low viscosity ratio where the temperature difference across the layer is least (Krishnamurti 1968).

Detection of R_{0c} presents several practical problems. Figure 11 also shows measurements of N at $c = 5{\cdot}0$. N is observed to jump about 10 % at onset. Extrapolation of values of N for $R > R_{0c}$ back to $N = 1$ as is usual for constant viscosity would give R_{0c} 20 % below its true value. It is therefore necessary to directly observe the jump in N at R_{0c}. Unfortunately the experimental scatter in N exceeds the jump for $c < 5$, and reliable determination of R_{0c} from the Nusselt-number measurements is not possible.

We therefore used the appearance of the convective pattern on the shadowgraph screen to detect onset. Because of the large temperature difference across the fluid ($\Delta T > 20\,^\circ$C) and the finite amplitude of the initial convection, there is little danger of over-estimating ΔT_c because the amplitude at critical is too small to observe. The vertical solid line in figure 11 is drawn at R_0^*, the value of R_0 at which the pattern is first observed, interpolated from an experimental run in which appearance of the pattern was the only criterion for onset. It is clear that the visual onset is in excellent agreement with the observed discontinuity in N. Over the full range of c, the visually determined R_0^* always lies within the uncertainty of the value of R_0 at which the jump in N occurs.

The observed pattern at onset was usually observed to be up-hexagons (up-flow in the centre). An experiment with very small viscosity variation ($c = 0{\cdot}12$) using silicone oil produced only concentric rolls. At small to moderate c in glycerol an initial pattern of rolls always broke up into hexagons after the apparatus had been allowed to sit with constant ΔT for several hours. The subsequent development of the pattern as R increased above R_{0c} is quite interesting, and is discussed in detail elsewhere (Oliver 1980, 1982). To summarize, however: For $c < 2$ the hexagons convert to rolls at an R that increases with c in excellent agreement with theoretical predictions of Busse (1967); for $c > 2$ the hexagons convert to irregular polygons at an R that decreases rapidly with increasing c so that the range of stability of hexagons becomes very small at large c; for $c \geqslant 4$ the polygons convert to squares with a modest further increase in R. Oliver finds that the large amplitude of the flow at R_{0c} precludes study of the square pattern by the methods of Busse (1967).

Observed values of R_0^* for $c = 2{\cdot}0$–$8{\cdot}1$ (viscosity ratios from 7–3400) are plotted as crosses in figure 12. However, R_0^* is not R_{0c}. The experiment regulates the temperature below the glass bottom. The increase in N as the convection begins increases the temperature drop across the glass plate, and hence decreases ΔT and R_0. The final equilibrium is ΔT^* and R_0^* which we measure. Convection continues in the layer in a finite-amplitude subcritical state. However, the actual critical temperature drop across the fluid prior to the increase in N is easily shown to be

$$\Delta T_c = \left(1 + \frac{N-1}{N_B+1}\right) \Delta T^*,$$

where $N-1$ is the jump in Nusselt number at R_{0c}, and $N_B = 7{\cdot}345$ is the ratio of the temperature drop across the fluid layer in a purely conductive state to that across the glass plate.

Figure 13 plots measured values of $(N-1)^{\frac{1}{2}}$ versus c. These are estimated by extrapolating subcritical values of N back to R_0^*. Plotting the square root of the jump in Nusselt number is motivated by the parabolic shape of the theoretical heat-flux relation in figure 11. Although the uncertainty is fairly high, the straight line

$$(N-1)^{\frac{1}{2}} = 0{\cdot}0635c \tag{20}$$

is an excellent fit to the most-probable values. This relation slightly underestimates the jump at R_{0c} because $R_0^* < R_{0c}$. However, this error is small compared with the experimental uncertainty.

The calculated values of R_{0c} using (20) are shown as circles in figure 13. The correction to R_0^* is only $3 \pm 1\,\%$ at $c = 5$, but rises to $15 \pm 3\,\%$ at $c = 8{\cdot}1$.

The experimental points should be compared to the solid theoretical curve in figure 12. This curve assumes that α and c_p vary with temperature according to (17) and (18), and that T_0 varies with c in the same way as in the experiment. The variation of T_0 is included because the non-dimensional fluid property functions f, A and Q derived from (19), (17) and (18) depend on the actual value of T_0. Fortunately, T_0 in the experiments decreases smoothly as c increases, so that the calculated values of R_{0c} remain on a smooth curve. The dashed theoretical curve in figure 12 assumes that α and c_p are constant, and is shown for comparison. The difference between the two theoretical curves grows as c increases, and exceeds 10 % for $c > 6$. It is worth noting that this correction can be calculated quite accurately ($< 10\,\%$) by evaluating α and

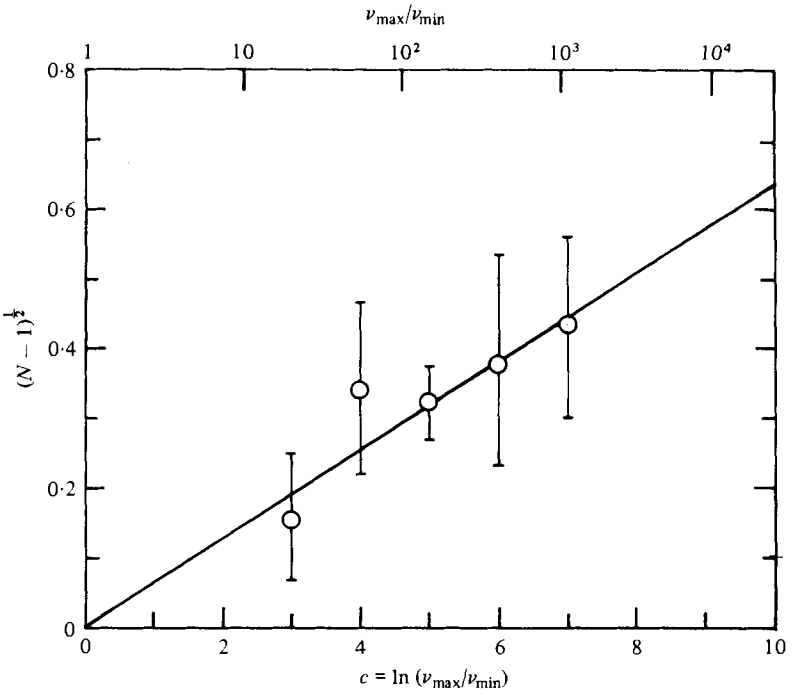

FIGURE 13. Square root of the measured jump in Nusselt number N at R_0^* versus viscosity ratio. The line is relation (20).

c_p at $\bar{T}(z_p)$, the temperature at the peak of the vertical velocity eigenfunction, rather than at T_0. The theoretical calculations also take into account the finite conductivity of the lower boundary in the experimental apparatus and therefore have a lower R_{0c} at constant viscosity than with a perfectly conducting boundary. This lowering of R_{0c} depends only on N_B.

Our estimated uncertainties in the properties of glycerol plus the 0·25 % uncertainty in the layer depth could account for up to $\pm$ 7 % c-independent uncertainty in the experimental values of R_{0c}. The actual mean difference between theory and experiment is only 2 %, with a maximum difference less than 4 %. The trend of the differences with c can be adequately accounted for either by the uncertainty in the correction for the finite jump in N or the uncertainty in the temperature gradient of the thermal expansion coefficient α.

8. Conclusions

Liquids have a viscosity that decreases with increasing temperature and that typically can be well-approximated by an exponential or super-exponential function with a steeper viscosity gradient at low temperatures. We find for these fluids that the theoretical critical Rayleigh number R_{0c} based on the viscosity at the mean of the boundary temperatures increases as the ratio between the boundary viscosities initially increases. If the logarithmic temperature derivative of the viscosity is sufficiently negative, R_{0c} reaches a maximum at a critical viscosity ratio. In the large-viscosity-ratio regime above this critical viscosity ratio, R_{0c} decreases, and the onset of convection is governed by a sublayer that is more unstable than the full layer.

A lower effective viscosity within this sublayer outweighs the stabilizing effect of the sublayer's reduced thickness.

For fluids with an exponential viscosity variation, the critical viscosity ratio is 2981. At higher viscosity ratios, convection begins first in the sublayer that has a viscosity ratio equal to this critical value. The fluid above the sublayer can be considered stagnant, and the structure of the convection within the sublayer remains constant with respect to the thickness of the sublayer. In particular, the half-wavelength of the convection always equals the sublayer depth. Our calculations for glycerol lead to essentially the same conclusions, although the critical viscosity ratio is somewhat higher.

Our numerical results for exponential and super-exponential viscosity variations are in clear contrast to the calculation by Liang (1969) for a fluid similar to glycerol, and to the work of Palm (1960) and Jenssen (1963) for a fluid with a cosine viscosity variation. All these workers find a decrease of R_{0c} as the viscosity ratio increases. It is clear now that Liang's work is in error. Palm and Jenssen's results are correct, but not relevant to real liquids. Not only is the direction of change in R_{0c} different at small viscosity ratio, but the structure of the convection at large viscosity ratio is fundamentally different. The stagnation of the upper part of the layer and the confinement of the initial convection to a sublayer never occurs with the cosine viscosity variation. Furthermore, the cosine variation develops a thin slippery region at the bottom boundary which makes results for rigid and free lower boundaries nearly identical at large viscosity ratio. This behaviour is opposite to the exponential fluid and glycerol. Although the cosine viscosity variation has useful properties for theoretical calculations, it is clear that one must be extremely careful about applying results derived from this model to real liquids.

Our experiment with glycerol confirms the initial increase of R_{0c} with viscosity ratio. As the viscosity ratio becomes large, however, accurate determination of R_{0c} when the boundaries are not infinitely conducting requires accounting for the effect of the finite discontinuity in heat transport at R_{0c} on the measured boundary temperatures. We observe a maximum R_{0c} 33 % above the constant-viscosity value of a viscosity ratio of about 1200. At higher viscosity ratios, the measured R_{0c} decreases.

For our glass-bottomed apparatus, numerical calculations with constant thermal expansion coefficient and specific heat predict a maximum R_{0c} 48 % above the constant-viscosity value at a viscosity ratio of about 2500. The maximum viscosity ratio of 3400 reached in our experiment is barely in the large-viscosity regime. The measured maximum and subsequent decrease in R_{0c} is not due to the formation of the sublayer but is a result of the temperature dependence of the thermal expansion coefficient and specific heat. Numerical calculations including the empirical temperature-dependence of the thermal properties of glycerol predict values of R_{0c} in excellent agreement with the experiment. We conclude that the linear stability analysis is valid despite the non-existence of an infinitesimal-amplitude state at R_{0c}.

This work was supported by the National Science Foundation under Grants no. EAR75-21793 and EAR78-23409.

REFERENCES

BOOKER, J. R. & STENGEL, K. C. 1978 Further thoughts on convective heat transport in a variable viscosity fluid. *J. Fluid Mech.* **86**, 289.

BUSSE, F. H. 1967 The stability of finite amplitude cellular convection and its relation to an extremum principle. *J. Fluid Mech.* **30**, 625.

BUSSE, F. H. & WHITEHEAD, J. A. 1971 Instabilities of convection rolls in a high Prandtl number fluid. *J. Fluid Mech.* **47**, 305.

HOARD, C. Q., ROBERTSON, C. R. & ACRIVOS, A. 1970 Experiments on the cellular structure in Bénard convection. *Int. J. Heat Mass Transfer* **13**, 849.

JENSSEN, O. 1963 Note on the influence of variable viscosity on the critical Rayleigh number. *Acta Polytech. Scand.* **24**, 1.

KRISHNAMURTI, R. 1968 Finite amplitude convection with changing mean temperature. Part 1. Theory. *J. Fluid Mech.* **33**, 440.

LIANG, S. F. 1969 Ph.D. dissertation, Stanford University.

NEWMAN, A. A. 1968 *Glycerol.* CRC Press.

OLIVER, D. S. 1980 Bénard convection with strongly temperature-dependent viscosity. Ph.D. dissertation, University of Washington.

OLIVER, D. S. 1982 Experimental study of convection with strongly temperature-dependent viscosity (unpublished manuscript).

PALM, E. 1960 On the tendency towards hexagonal cells in steady convection. *J. Fluid Mech.* **8**, 183.

PELLEW, A. & SOUTHWELL, R. V. 1940 On maintained convective motion in a fluid heated from below. *Proc. R. Soc. Lond.* A **176**, 312.

RICHTER, F. M. 1978 Experiments on the stability of convection rolls in fluids whose viscosity depends on temperature. *J. Fluid Mech.* **89**, 553.

SCHMIDT, R. J. & MILVERTON, S. W. 1935 On the instability of a fluid when heated from below. *Proc. R. Soc. Lond.* A **152**, 586.

SEGUR, J. B. & OBERSTAR, H. E. 1951 The viscosity of glycerol and its aqueous solutions. *Ind. Engng Chem.* **43**, 2117.

SCHUBERT, G., TURCOTTE, D. L. & OXBURGH, E. R. 1969 Stability of planetary interiors. *Geophys. J. R. Astron. Soc.* **18**, 441.

SILVESTON, P. L. 1958 Wärmedurchgang in waagerechten Flüssigkeitschichten. *Forsch. Ing. Wes.* **24**, 59.

SOMERSCALES, E. F. C. & DOUGHERTY, T. S. 1970 Observed flow patterns at the initiation of convection in a horizontal liquid layer heated from below. *J. Fluid Mech.* **42**, 755.

STENGEL, K. C. 1977 Onset of convection in a variable viscosity fluid. M.S. thesis, University of Washington.

TAMMAN, V. G. & HESSE, W. 1926 Die Abhängigkeit der Viscosität von der Temperatur bei unterkühlten Flüssigkeiten. *Z. anorg. allg. Chem.* **156**, 245.

TORRANCE, K. E. & TURCOTTE, D. L. 1971 Thermal convection with large viscosity variations. *J. Fluid Mech.* **47**, 113.